Kelvin wave signatures in ECMWF meteo fields and Global Ozone Monitoring Experiment (GOME) ozone columns

R. M. A. Timmermans, R. F. van Oss, and H. M. Kelder[1]

Royal Netherlands Meteorological Institute, De Bilt, Netherlands

Received 21 July 2004; revised 4 February 2005; accepted 23 February 2005; published 1 July 2005.

[1] This study investigates the vertical structure of the Kelvin wave signals previously found in total ozone column measurements from the Global Ozone Monitoring Experiment (GOME) instrument. For this, zonal wind and temperature measurements from the European Centre for Medium-Range Weather Forecasts (ECMWF) Re-Analysis data set are analyzed by using the same bidimensional spectral method as was used to analyze the GOME total ozone columns. These fields are available on 60 levels from the surface to 0.1 hPa. For the three high Kelvin wave activity periods identified in the GOME data we found spectral features in the ECMWF fields associated with Kelvin waves with zonal wave numbers 1 or 2 and periods around 15–20 days. These characteristics correspond to the characteristics of the Kelvin waves detected in GOME. The signals are significant throughout the lower stratosphere between ~100 and 10 hPa and, depending on the period, are largest around 15, 45, or 65 hPa. There is a good correlation between the Kelvin wave signals in the ECMWF zonal wind and temperature and the GOME total ozone column. The induced fluctuations in zonal wind and temperature are, respectively, up to 8 m/s and 2 K. From these induced zonal wind fluctuations, expected total ozone column fluctuations of around 1 DU are calculated, corresponding to the ozone fluctuations found in the GOME data. The results indicate that the analyzed total ozone column fluctuations are mainly caused by transport effects in the lower stratosphere. This study shows that combined use of ECMWF Re-Analysis data and GOME ozone columns provides a possibility to study the three-dimensional structure of Kelvin wave activity.

Citation: Timmermans, R. M. A., R. F. van Oss, and H. M. Kelder (2005), Kelvin wave signatures in ECMWF meteo fields and Global Ozone Monitoring Experiment (GOME) ozone columns, *J. Geophys. Res.*, *110*, D13104, doi:10.1029/2004JD005261.

1. Introduction

[2] Equatorial Kelvin waves play a significant role in the dynamics of the middle atmosphere. The main forcing mechanism of these waves is likely the latent heat release in large-scale deep convection [*Holton*, 1992]. The waves propagate vertically and zonally in eastward direction through the atmosphere, and in this way can carry momentum into the middle and upper atmosphere. This process is believed to play a large role in the driving of the quasi-biennial oscillation (QBO) of the zonal mean winds in the lower stratosphere and the semi-annual oscillation (SAO) in the upper stratosphere and mesosphere. Kelvin waves are also thought to play a role in the stratospheric dehydration mechanism [*Fujiwara et al.*, 2001; *Fujiwara and Takahashi*, 2001] and the transport of stratospheric ozone into the troposphere [*Fujiwara et al.*, 1998].

[1]Also at Eindhoven University of Technology, Eindhoven, Netherlands.

0148-0227/05/2004JD005261$09.00

[3] A Kelvin wave modulates geopotential height, zonal velocity and vertical velocity, and also temperature through the diabatic heating and cooling of the vertical displacements. The Kelvin wave also induces fluctuations in the ozone concentration. In the lower stratosphere, where ozone has a strong vertical gradient and a long photochemical lifetime, the ozone perturbations are mainly controlled through the velocity modulations. Conversely, in the upper stratosphere, ozone has a short chemical lifetime and a temperature-dependent equilibrium concentration. The ozone fluctuations in this part of the atmosphere are therefore mainly controlled by the temperature dependence of the photochemical reactions.

[4] *Wallace and Kousky* [1968] were one of the first to observe Kelvin waves in the atmosphere. They used wind and temperature measurements from radiosondes and identified Kelvin waves in the lower stratosphere with periods of about 2 weeks, referred to as "slow Kelvin waves." Later on, several studies have analyzed Kelvin waves in wind, temperature, and ozone profile measurements by both ground-based and satellite instruments. In these studies, distinction is made between "ultra-slow," "slow," "fast," and "ultra-fast" Kelvin waves with phase speeds of

respectively ∼10–20 m/s, ∼25–30 m/s, ∼70 m/s, and ∼120 m/s. Satellite observations allow the investigation of the global structure of Kelvin waves. Fast Kelvin waves were identified in the temperature and ozone measurements from the Limb Infrared Monitor of the Stratosphere (LIMS) and Solar Backscatter Ultraviolet (SBUV) instruments on board the Nimbus-7 spacecraft [*Salby et al.*, 1984, 1990; *Randel*, 1990; *Randel and Gille*, 1991] and the Improved Stratospheric And Mesospheric Sounder (ISAMS) [*Stone et al.*, 1995] and Microwave Limb Sounder (MLS) [*Canziani et al.*, 1994, 1995; *Mote and Dunkerton*, 2002] on board the Upper Atmosphere Research Satellite (UARS). Slow Kelvin waves in the lower stratosphere need observations with a sufficiently high vertical resolution to get resolved. They have been observed in temperature and ozone profiles retrieved from measurements by LIMS [*Kawamoto et al.*, 1997], MLS [*Mote and Dunkerton*, 2004], and Cryogenic Limb Array Etalon Spectrometer (CLAES) [*Shiotani et al.*, 1997; *Canziani*, 1999; *Mote and Dunkerton*, 2004], the latter two on board UARS. The limited (continuous) time periods covered by the LIMS, MLS, and CLAES measurements do not, however, allow the study of the variability of slow Kelvin waves over more than 2 years and by that the conjunction with the QBO cycle. The studies [e.g., *Kawamoto et al.*, 1997; *Mote and Dunkerton*, 2004] that treat ozone Kelvin waves show dominant ozone mixing ratio variations at the level where the vertical gradient in zonal mean ozone is largest. These variations are attributed to dynamical advection of ozone and are in phase with temperature variations. A second maximum in ozone variability due to Kelvin waves is often found in the upper stratosphere, attributable to photochemical perturbations. These variations show an out of phase relationship with temperature variations.

[5] *Ziemke and Stanford* [1994] showed that also total column measurements of ozone are sensitive to "slow Kelvin waves" in the stratosphere. They found Kelvin wave signatures in the Nimbus-7 TOMS (Total Ozone Mapping Spectrometer) data.

[6] In a previous study, *Timmermans et al.* [2004] (hereinafter referred to as T04) demonstrated that GOME (Global Ozone Monitoring Experiment) ozone column measurements also exhibit features that can be attributed to tropical Kelvin waves. By introducing bidimensional unequally spaced data spectral analysis, we analyzed 7 years of GOME data and identified three periods of high Kelvin wave activity. The induced Kelvin wave signatures in the ozone concentrations of 2–4 DU peak-to-peak correspond to eastward propagating waves 1–2 with periods of 12–15 days. These results agree with the characteristics of "slow" Kelvin waves in the lower stratosphere. However, no additional vertical information on the Kelvin waves can be retrieved from the total column ozone measurements themselves.

[7] To acquire more information on the vertical structure of the Kelvin waves, we will in this study correlate the variations in the GOME total column ozone data to variations in the European Centre for Medium-Range Weather Forecasts (ECMWF) Re-Analysis (ERA-40) zonal wind and temperature data, available at different altitudes. We will first analyze the ERA-40 data in the three high Kelvin wave activity periods identified in the ozone column data. Using these analyses, we will compute the expected total ozone column perturbations and compare these with the ozone column perturbations found in T04.

2. Data and Analysis

2.1. GOME

[8] The Global Ozone Monitoring Experiment (GOME) instrument is a nadir-viewing spectrometer on board the second European Remote Sensing Satellite (ERS-2), which was launched on 21 April 1995. From the measured radiance and irradiance spectra, total ozone column values are retrieved with a global coverage in 3 days. The spatial resolution is 40 km in latitudinal and 320 km in longitudinal direction. For a more extensive description of the GOME data and its accuracy, we refer to T04 and references therein.

2.2. ECMWF Re-Analysis Data Set, ERA-40

[9] The ECMWF ERA-40 data set consists of a set of global fields describing the state of the atmosphere (the "analysis"). These fields are produced by combining atmospheric observations with a forecast model using data assimilation [*Simmons and Gibson*, 2000]. The data set covers the period from September 1957 to August 2002. The observations come from a wide selection of sources: radiosondes, aircraft, and ground-based and satellite instruments, each of these measurements with their own accuracy. To obtain a complete representation at all locations and times, the measurements are combined with results from a short-range forecast initiated from the preceding analysis. The observations and forecast are then combined using estimates of the statistics of their errors to form the new analysis. Every 6 hours a new analysis is made.

[10] For this study we use the temperature and zonal and meridional wind fields from the ERA-40 data set. We retrieved these three fields from the ECMWF data set on a 5° × 5° grid (resolution of original data T159) and average over 3 days (if not stated otherwise) to match the used GOME ozone fields. From this grid we have subsequently focused on the latitude band between 2.5°S and 2.5°N because Kelvin waves reach maximum amplitude at the equator. All results presented below are for this latitude band. The fields are available on 60 levels between the surface and 0.1 hPa. The vertical resolution is highest in the planetary boundary layer and lowest in the stratosphere and lower mesosphere. The model levels are calculated in relation to the surface pressure. An example of the pressure on the 60 levels for a surface pressure of 1015 hPa is given in Table 1.

[11] Between 40 and 4 hPa the level spacing is precisely 1.5 km. In the lower stratosphere, the level spacing is between 1 and 1.5 km. This vertical resolution should be sufficient for the detection of slow Kelvin waves, considering typical vertical wavelengths of these waves of about 8–10 km.

[12] *Tindall* [2003] and *Tindall et al.* [2005b] investigated the representation of equatorial waves in ERA-15 data. In this study it is demonstrated that the Kelvin wave activity in the ERA-15 data show seasonal and interannual variations consistent with previous studies using other data sources. For example, maximum Kelvin wave activity at 50 hPa coincides with the change in the zonal wind at this altitude

Table 1. ERA-40 Pressure Levels for a Surface Pressure of 1015 hPa

Level	Pressure, hPa
1	0.1
2	0.3
3	0.5
4	0.8
5	1.2
6	1.6
7	2.1
8	2.7
9	3.4
10	4.2
11	5.2
12	6.4
13	8
14	9.8
15	12
16	15
17	19
18	23
19	29
20	36
21	44
22	55
23	67
24	80
25	96
26	113
27	133
28	154
29	177
30	202
31	229
32	257
33	288
34	320
35	353
36	388
37	425
38	462
39	500
40	538
41	577
42	616
43	654
44	691
45	728
46	763
47	797
48	828
49	857
50	884
51	908
52	930
53	949
54	965
55	979
56	989
57	998
58	1004
59	1009
60	1012

from easterlies to westerlies. This is consistent with the results from *Shiotani et al.* [1997] and references therein. Other studies have found equatorial waves in ERA-15 to be representative of the atmosphere. *Straub and Kiladis* [2002], for example, found Kelvin wave signals in ERA-15 in agreement with signals in radiosonde data. Furthermore, *Pawson and Fiorino* [1998] found a good agreement in the annual temperature cycle at 100 and 70 hPa between data from ERA-15 and radiosondes. All these studies give an indication of the reliability of ERA-15 data in terms of Kelvin waves. Although in this study we are using ERA-40 data instead of ERA-15, the conclusions from these studies are expected to be similar for the ERA-40 data. The main changes in ERA-40 compared to ERA-15 are the length of the data set (40 years instead of 15) and the improved vertical resolution. This improved vertical resolution should be advantageous for the detection of Kelvin waves.

2.3. Analysis Method

[13] In this study we have used the bidimensional spectral analysis method introduced in T04. This method can handle unequally spaced data, such as satellite data containing gaps, without making use of interpolation techniques, which can introduce spurious peaks in the power spectrum. The simple statistical behavior of the method, allowing easy determination of the statistical significance of an observed feature, is another important advantage of the method.

[14] The spectral method is based on the Lomb periodogram [*Press et al.*, 1992; *Scargle*, 1982]. In T04 this periodogram is extended from one to two dimensions so as to allow its application to the bidimensional GOME data (as function of longitude and time). The periodogram gives an indication of the dominant frequencies in a data set. For each level in the ERA-40 data separately, we calculate the extended Lomb normalized periodogram as function of angular frequency ω and zonal wave number k.

3. Linear Kelvin Wave Theory

[15] In this section we will derive the solutions for Kelvin wave induced perturbations in zonal wind, geopotential height, and temperature using linear wave theory. Following *Andrews et al.* [1987], the basic equations for describing equatorial waves are given by

$$\frac{\partial u'}{\partial t} - \beta y v' + \frac{\partial \Phi'}{\partial x} = 0, \quad (1)$$

$$\frac{\partial v'}{\partial t} + \beta y u' + \frac{\partial \Phi'}{\partial y} = 0, \quad (2)$$

$$\frac{\partial u'}{\partial x} + \frac{\partial v'}{\partial y} + \rho_0^{-1} \frac{\partial(\rho_0 w')}{\partial z} = 0, \quad (3)$$

$$\frac{\partial \Phi'}{\partial z} = H^{-1} R T'. \quad (4)$$

The primes denote wave perturbations in zonal wind u, meridional wind v, vertical velocity w, geopotential height Φ, and temperature T; ρ_0 is the standard density, R is the gas constant for dry air (= 287 JK^{-1} kg^{-1}), and H is the scale height, which is $\approx$7 km in the middle atmosphere. Here x, y, and z are, respectively, the longitudinal, zonal, and vertical coordinates.

[16] These equations are derived from the linearized momentum balance, continuity, and hydrostatic balance

equations, neglecting nonconservative processes. All field variables are split up into a time- and longitude-averaged mean, indicated with an overbar and a wave perturbation, for example, $u = \bar{u} + u'$. Here $\bar{u}$ is set to zero. Since we are dealing with latitudinally confined waves, the equatorial β-plane approximation has been used in which the Coriolis parameter f is replaced by βy ($\beta = 2\Omega a^{-1}$, a is the Earth's radius, and y is the distance north of the equator).

[17] Solutions to equations (1)–(4) can be written in the form

$$(u', v', w', \Phi') = e^{z/2H} Re\left[\left(\hat{u}(y), \hat{v}(y), \hat{w}(y), \hat{\Phi}(y)\right) \cdot \exp\ i(kx + mz - \omega t) \right]. \tag{5}$$

Here k and m are the zonal and vertical wave numbers, respectively, and ω is the frequency. Different solutions can be found for ($\hat{u}(y)$, $\hat{v}(y)$, $\hat{w}(y)$, $\hat{\Phi}(y)$) which satisfy equations (1)–(4). The simplest one where we take $\hat{v} = 0$ concerns the Kelvin wave. In this case, $\hat{u}$ and $\hat{\Phi}$ have to satisfy the following relationships:

$$-\omega \hat{u} + k\hat{\Phi} = 0, \tag{6}$$

$$\beta y \hat{u} + \hat{\Phi}_y = 0, \tag{7}$$

$$k\hat{u} - \omega N^{-2}\left(m^2 + \frac{1}{4H^2}\right)\hat{\Phi} = 0. \tag{8}$$

These relationships are derived by substituting equation (5) into equations (1)–(4) and using $\rho_0 = \rho_s e^{z/H}$, where ρ_s is the density at the surface. The buoyancy frequency N is defined as

$$N^2 = \frac{R}{H}\left[\frac{\partial T}{\partial z} + \frac{\kappa T}{H}\right], \tag{9}$$

with $\kappa = R/c_p$, and c_p is the specific heat at constant pressure.

[18] The meridional structure of this wave solution can be found by combining equations (6) and (7),

$$\hat{\Phi}(y) = \hat{\Phi}_0\ \exp\left(-\beta k y^2/2\omega\right), \tag{10}$$

where $\hat{\Phi}_0$ is the amplitude of the wave in geopotential height at the equator and $z = 0$. The wave solutions are then given by [*Tindall*, 2003; *Tindall et al.*, 2005a]

$$u' = \frac{k}{\omega}\ \hat{\Phi}_0\ \exp\left(-\beta k y^2/2\omega\right) e^{z/2H} Re[\ \exp\ i(kx + mz - \omega t)], \tag{11}$$

$$\Phi' = \hat{\Phi}_0\ \exp\left(-\beta k y^2/2\omega\right) e^{z/2H} Re[\ \exp\ i(kx + mz - \omega t)], \tag{12}$$

$$T' = \frac{H}{R}\ \hat{\Phi}_0\ \exp\left(-\beta k y^2/2\omega\right) e^{z/2H} Re \cdot \left[\ \left(\frac{1}{2H} + im\right)\ \exp\ i(kx + mz - \omega t)\right]. \tag{13}$$

The latter one is derived from the hydrostatic equation (4). For a Kelvin wave with $|m| \gg \frac{1}{2H}$, temperature perturbations will lead the zonal wind perturbations by one quarter of a cycle. This so-called "Boussinesq" approximation is reasonable for "slow" Kelvin waves in the lower stratosphere.

[19] From equations (6) and (8) we get $\omega = \pm Nkm^{-1}$ and the vertical group velocity $c_g^{(z)} \equiv \partial\omega/\partial m = \mp N\ km^{-2}$. For an upward propagating Kelvin wave the positive $c_g^{(z)}$ will be the physical solution and the dispersion relationship is given by

$$\omega = -Nk/m. \tag{14}$$

[20] Equations (1)–(4) are valid for $\bar{u} = 0$. For a nonzero but constant $\bar{u}$, these equations are somewhat more extensive but the solutions (11)–(14) can be easily adapted by replacing ω with the intrinsic frequency $\omega^+ = \omega - ku$.

4. Results

[21] In the previous study, T04, we found in the GOME ozone column data three periods of high Kelvin wave activity: P1 from 15 July to 13 September 1996, P2 from 17 July 1998 to 15 September 1998, and P3 from 19 September 2000 to 18 November 2000. These three periods correlate with periods of westward zonal winds in the lower stratosphere as can be seen in Figure 1. Below we show the results of the analyses of the ERA-40 zonal wind and temperature data concentrating on these three periods.

4.1. P1: 15 July to 13 September 1996

[22] Figure 2 shows the periodogram P_N as function of wave number and period for the ECMWF temperature and zonal and meridional wind velocity at 15 hPa calculated over the 60-day time period from 15 July to 13 September 1996. This time period corresponds to the time period P1 in T04.

[23] In both the temperature and zonal wind field, one large significant eastward signal is found. This significant signal is located at wave numbers 1 and 2 with periods around 15–20 days. This maximum corresponds to the signal found in the GOME total ozone data in T04 and agrees with Kelvin wave characteristics. The meridional wind field does not show a significant signal at these wave numbers and periods, another indication that the signal is Kelvin wave related, since Kelvin waves do not have a meridional component. The signal is also present in the periodograms of the temperature and zonal wind at other altitudes between approximately 100 and 7 hPa, as can be seen in Figure 3. The signal in zonal wind is largest at ~20 hPa and in temperature at 35 hPa for wave periods of 20 days and 15 hPa for wave periods of 15 days.

[24] Figure 4 shows Hovmöller diagrams (time versus longitude plots) for the temperature and zonal and meridional wind fields at 15 hPa from 15 July to 13 September 1996. To produce this figure we used the daily values instead of the 3-day averaged values. The data are filtered so as to preserve only the dominant frequencies found in the temperature and zonal wind periodograms that are expected to arise from Kelvin waves. The filter only retains wave numbers 1 and 2. In time a band-pass filter given by *Murakami* [1979] is applied with half amplitudes at 12

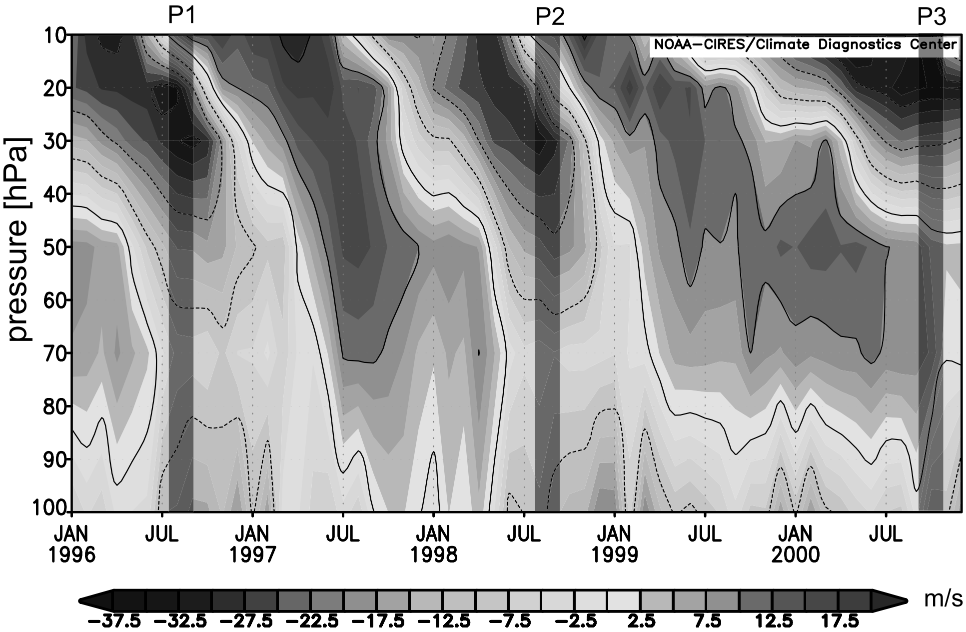

Figure 1. Monthly mean zonal wind (m/s) at the equator and 105° E for January 1996 to December 2000 and pressure levels between 100 and 10 hPa. (Image provided by the NOAA-CIRES Climate Diagnostics Center, Boulder, Colorado, USA, from their Web site at http://www.cdc.noaa.gov/.) See color version of this figure at back of this issue.

and 20 days. From these figures we can retrieve the amplitudes of the wave perturbations in the wind velocity and temperature. At this level, observed perturbations in the zonal wind are up to 8 m/s and in the temperature are ~2 K. The perturbations in the meridional wind are negligible as expected from Kelvin wave theory. These values agree with the observed values given by *Andrews et al.* [1987]. The wave period and phase speed determined from these Hovmöller diagrams are, respectively, 15 days and 31 m/s, which agrees with the characteristics of the slow Kelvin wave in the lower stratosphere.

[25] Taking a cross section of these plots at a fixed time, as shown in Figure 5 for 10 September 1996, provides an image of the phase difference in space between the zonal wind and temperature perturbations. It can be seen that the zonal wind lags the temperature perturbations by a one-quarter cycle, which corresponds to the linear Kelvin wave theory explained in section 3. The $\partial T/\partial x$ is thus in phase

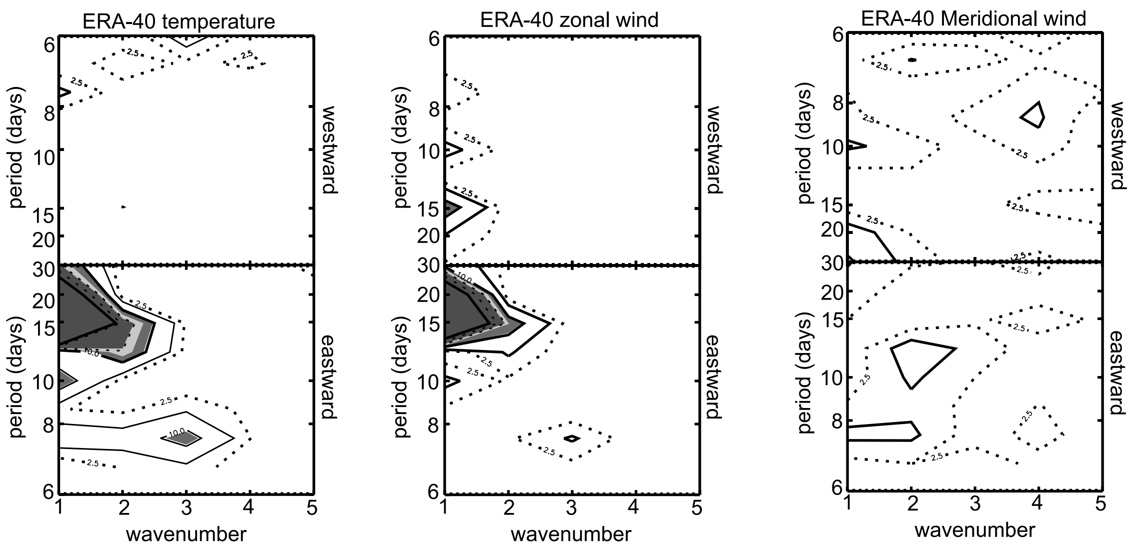

Figure 2. Lomb periodogram for ERA-40 temperature and zonal and meridional wind at 15 hPa for the period 15 July to 13 September 1996. Contour lines start at 2.5, followed by contour lines at 5, 10, 15, 20 and 25. The blue, green, and red areas, respectively, denote the 90%, 99%, and 99,9% significant signals. See color version of this figure at back of this issue.

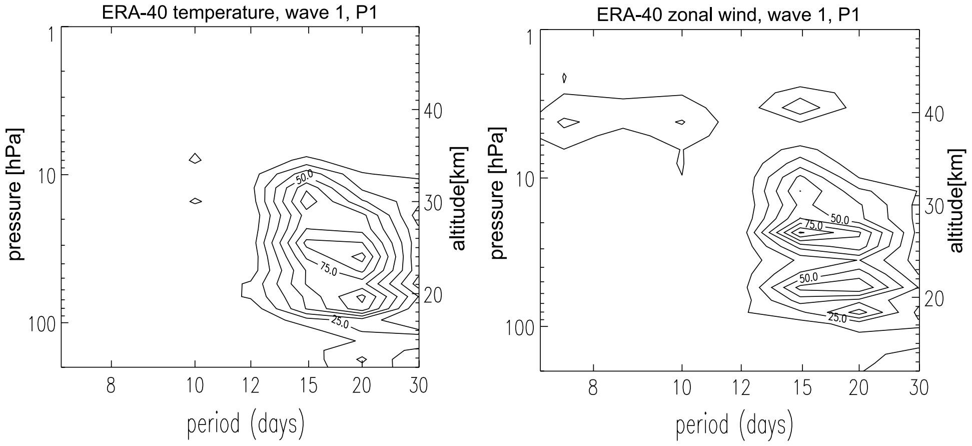

Figure 3. Lomb periodogram for ERA-40 temperature and zonal wind, for eastward waves with zonal wave number 1 for the period 15 July to 13 September 1996.

with the zonal wind perturbations as can be seen in this figure.

[26] Figures 6 and 7 show pressure versus longitude and pressure versus time plots for the temperature and zonal wind perturbations, respectively, on 23 August 1996 and at longitude = 310°, the date and longitude where we found our maximum zonal wind perturbation. A distinct wave 1 structure can be seen from approximately 200 to 5 hPa with an eastward phase tilt with height, characteristic for eastward moving Kelvin waves. Observed perturbations in these figures are up to 7 m/s for the zonal wind and 2K for the temperature, with largest values found between 10 and 20 hPa. Note that the largest amplitudes here are smaller than seen in the Hovmöller diagrams (Figure 4), this is caused by the 3-day averaging of the data here compared to the daily values used for producing the Hovmöller diagrams. Perturbations can also be seen below 200 hPa and above 5 hPa. These perturbations, however, do not show an eastward phase tilt with height and therefore cannot be attributed to Kelvin waves.

[27] Figure 8, a cross section of the pressure versus longitude plots, shows the vertical structure of the zonal wind and temperature perturbations. The data are not filtered in the vertical direction; nevertheless, a clear vertical wave structure can be seen in both the temperature and zonal wind plot, between approximately 100 hPa and 1 hPa, but note that above results showed that perturbations above 5 hPa cannot be attributed to Kelvin waves. The lower boundary is set by the tropopause region where the Kelvin waves originate and the upper boundary by the level where the waves dissipate. In the figure we can again see the one-quarter cycle phase difference between the temperature and zonal wind perturbations, this time in the vertical. The vertical wavelength derived from these plots is ~10 km. The amplitude of the fluctuations increases up to 10 hPa and decreases above 10 hPa. In the linear Kelvin wave theory

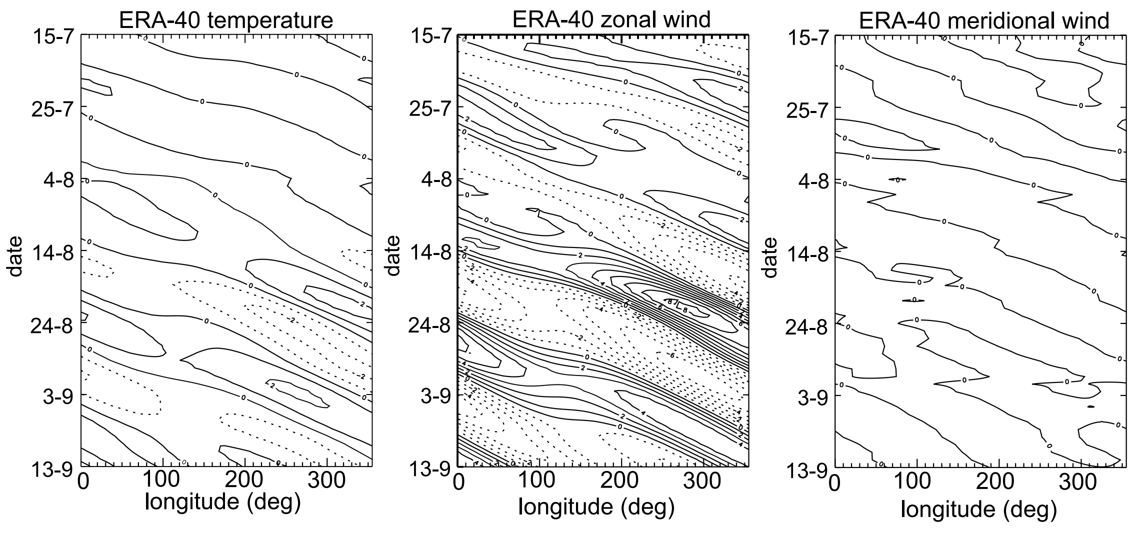

Figure 4. Hovmöller diagram of waves 1 and 2 in temperature and zonal and meridional wind velocity at 15 hPa. A band-pass filter with half amplitudes at 12 and 20 days has been applied. Solid lines start at zero K (for temperature) or m/s (for zonal and meridional wind) with increments of 1 for each contour line. Dashed lines start at −1 K or m/s with a decrement of 1 for each contour line.

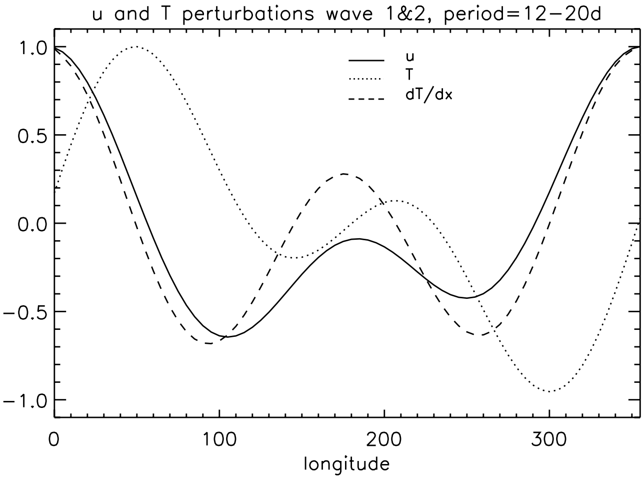

Figure 5. Normalized zonal wind (solid line) and temperature (dotted line) perturbations at 15 hPa on 10 September 1996 as function of longitude, filtered for wave 1 and 2 and with a band-pass filter with half amplitudes at 12 and 20 days. The dashed line is the derivative of the temperature perturbations in x direction (dT/dx).

the zonal wind is assumed constant. The $e^{(z/2H)}$ dependence on altitude is altered in case of a nonconstant zonal wind. *Andrews et al.* [1987] showed that Kelvin waves can only exist when their intrinsic phase velocity ($=c - \bar{u}_z$) is larger than zero and thus when the phase velocity is larger than the mean background zonal wind $\bar{u}_z$. In the presence of a vertical wind shear, the Kelvin waves will be able to propagate as long as $c > \bar{u}_z$ up to a critical level where $c = \bar{u}_z$. When approaching this critical level, the vertical wavelength and vertical group velocity will decrease and the waves become more susceptible to dissipation. This is what can be seen in Figure 8 around 10 hPa. The right plot in Figure 8 shows the mean zonal wind. The mean zonal wind becomes eastward between ~2.5 and 10 hPa and forms a critical level where dissipation of the waves take place. Above this level the Kelvin wave induced zonal wind and temperature perturbation are reduced. The signal in the periodograms of the temperature and zonal wind at wave numbers 1–2 and periods of 15–20 days was also diminishing at altitudes above ~10 hPa, pointing to dissipation of the waves at this altitude. Also, the decrease of vertical wavelength toward the critical level is visible in Figure 8. Large amplification of the amplitudes is observed in the region where westward winds change to eastward in agreement with previous studies [e.g., *Shiotani et al.*, 1997; *Tindall et al.*, 2005b].

[28] Figure 9 shows for 1996 the normalized ozone column periodogram and the normalized zonal wind and temperature periodograms, for wave 1 with a wave period of 15 days. The thick dashed lines are the periodogram values for the zonal wind and temperature on the 15-hPa level, which is the level where we found the largest temperature and zonal wind perturbations. The correlation coefficient between the ozone column periodogram and the zonal wind periodogram at 15 hPa is 0.63. The location of the peak in the ozone column periodogram coincides very well with the peak in the 15-hPa zonal wind and temperature periodograms. The 15-hPa zonal wind line follows the

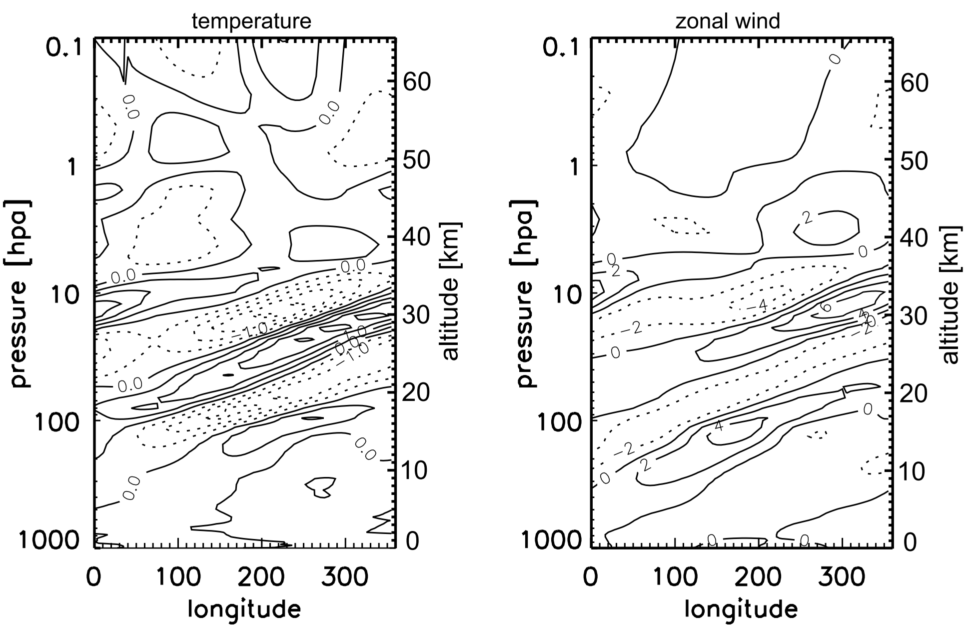

Figure 6. Pressure versus longitude plots of waves 1 and 2 in temperature and zonal wind velocity on 23 August 1996. A band-pass filter with half amplitudes at 12 and 20 days has been applied. Solid lines start at 0 K (for temperature) and 0 m/s (for zonal wind) with increments of 0.5 K and 2 m/s for each contour line. Dashed lines start at −0.5 K or −2 m/s with a decrement of 0.5 K and 2 m/s for each contour line.

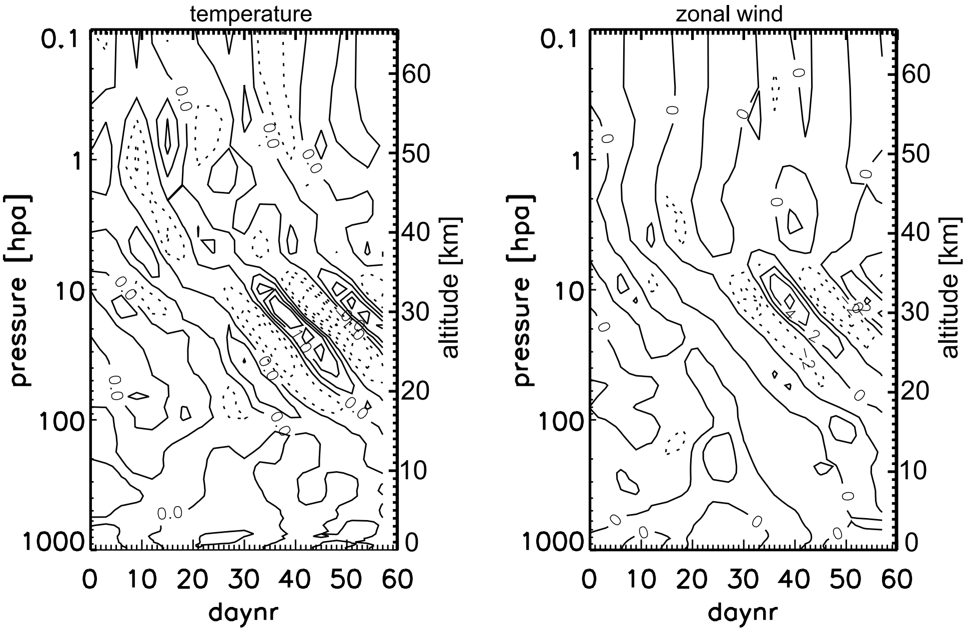

Figure 7. Pressure versus time (daynumber of the 60-day period 15 July to 13 September 1996) plots of waves 1 and 2 in temperature and zonal wind velocity at longitude = 310°. A band-pass filter with half amplitudes at 12 and 20 days has been applied. Solid lines start at 0 K (for temperature) and 0 m/s (for zonal wind) with increments of 0.5 K and 2 m/s for each contour line. Dashed lines start at −0.5 K or −2 m/s with a decrement of 0.5 K and 2 m/s for each contour line.

ozone line very well up until the peak mid-July 1996. After this peak the periodogram for the zonal wind is higher than for ozone; thus in the zonal wind at 15 hPa, there is more wave signal than in the ozone column. At some of the other altitudes, however, there is a lower wave signal after the peak than at 15 hPa. The correlation coefficient between the ozone column periodogram and the temperature periodogram at 15 hPa is 0.76. The 15-hPa temperature periodogram follows the ozone periodogram quite well from February until the peak in mid-July. After the peak

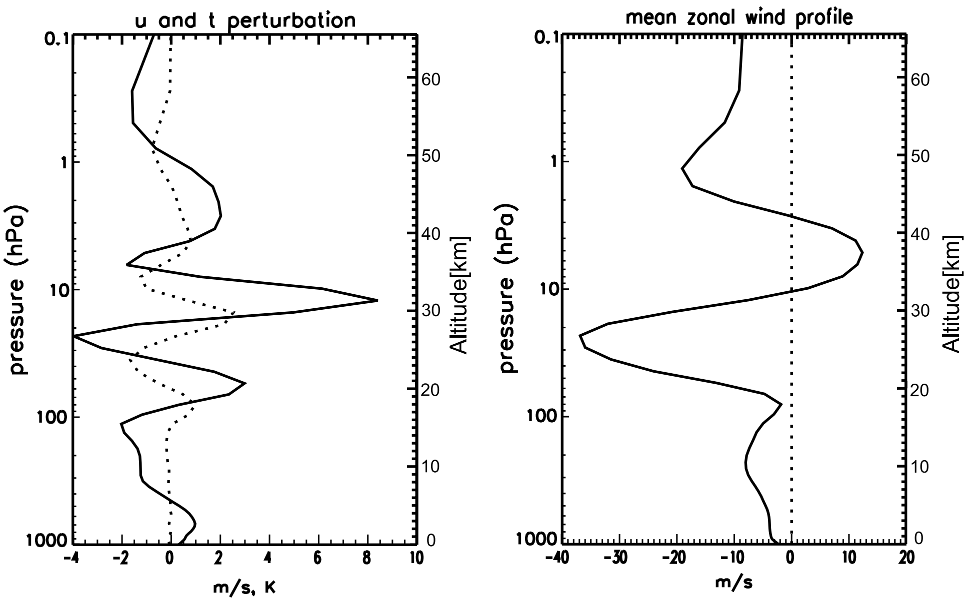

Figure 8. (left) Zonal wind and temperature perturbations of wave 1 and 2 as function of altitude on 23 August 1996 at longitude = 310°. The data are filtered in time with a band-pass filter with half amplitudes at 12 and 20 days. (right) Mean zonal wind profile over 60-day time period from 15 July to 13 September 1996 and all longitudes.

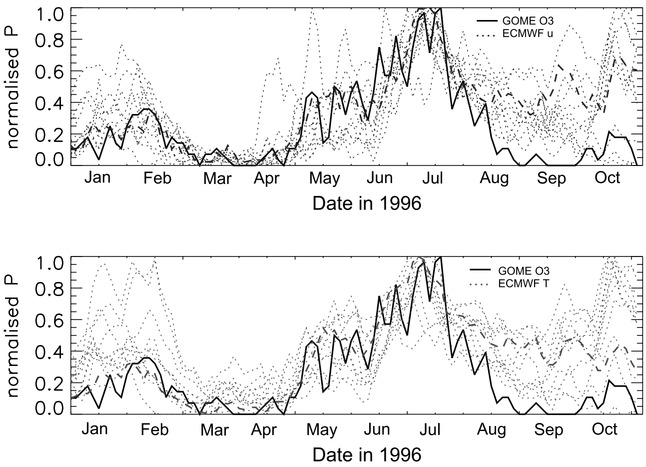

Figure 9. Normalized ozone column periodogram values P_N (solid line) and (top) normalized zonal wind and (bottom) temperature periodogram values, calculated over 60-day time periods, for wave 1 with a wave period of 15 days, as function of the starting day of the 60-day periods in 1996. The zonal wind and temperature periodograms are calculated on 11 different levels (dotted lines) between 80 hPa and 8 hPa. The thick dashed lines are the periodogram values on the 15-hPa level. See color version of this figure at back of this issue.

we see the same situation as in the zonal wind plot. Also in January the 15-hPa temperature periodogram lies above the ozone column line, but again some other altitudes show periodogram values closer to the ozone column ones. An explanation for this could be that a wave signal in the ozone column requires a wave signal in most levels between 80 and 10 hPa. Similar correlation plots have been analyzed for wave 1 with wave periods of 10, 12, 20, and 30 days. A good correlation was found between the zonal wind, temperature, and ozone column periodograms of waves with periods of 12 and 20 days. For the wave periods of 10 and 30 days the correlation was not very good.

[29] All the analyses shown here for P1 (15 July to 13 September 1996) have also been performed for the two other periods (17 July 1998 to 15 September 1998 and 19 September 2000 to 18 November 2000) in which we found high Kelvin wave activity in the GOME ozone column data.

4.2. P2: 17 July to 15 September 1998

[30] The results for P2 are somewhat similar to the results shown for the 1996 period. For P2 we found the maximum signal in the zonal wind and temperature periodograms of wave 1 with periods of 12–20 days at approximately 65 and 55 hPa (see Figure 10). The zonal wind and temperature periodograms at this level show a maximum around waves 1 and 2 with periods of 15 days, which is not present in the meridional wind.

[31] Figures 11 and 12 are the same as Figures 6 and 7 but now for, respectively, 10 August 1998 and longitude = 205°, the date and longitude where we find the largest Kelvin wave induced zonal wind perturbation. (Note that larger perturbations are found between 1.0 and 0.1 hPa; however, these perturbations do not show the characteristic eastward phase tilt with height and therefore cannot be attributed to Kelvin waves.) The Kelvin wave induced zonal wind and temperature perturbations between ~100 and 3 hPa are up to 3.8 m/s and 1.5 K, respectively. Largest perturbations are again found around 10–20 hPa; furthermore, large amplitudes can be found between 50 and 100 hPa, the altitude range where we found largest periodogram values. The vertical wavelength is about 10–12 km.

4.3. P3: 19 September to 18 November 2000

[32] The results are similar to the results shown for the P1 and P2 period. The maximum signal in the zonal wind and temperature periodograms of wave 1 with periods of 12–20 days are found around 15–20 hPa (see Figure 13). The periodogram also shows a significantly large signal at altitudes above 10 hPa. As can be seen in Figure 1, the mean zonal winds in P3 are strongest around 15–20 hPa compared to maximum winds around 30 hPa for periods P1 and P2. Therefore period P3 may be more favorable for wave propagation higher up in the stratosphere. The zonal

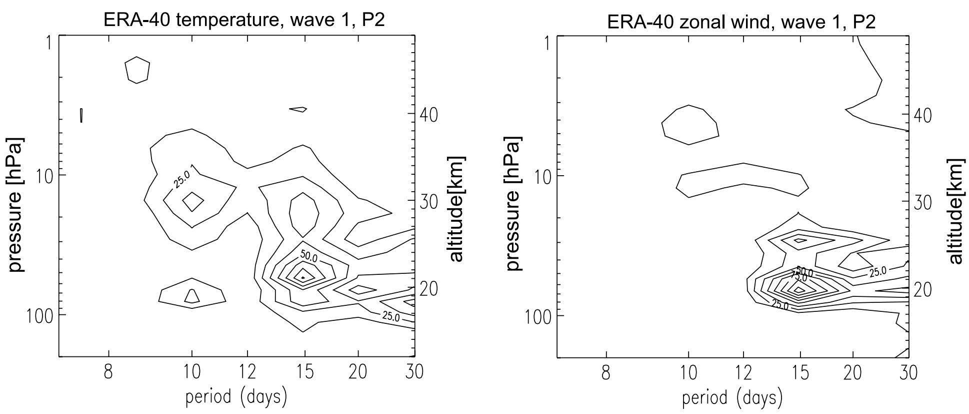

Figure 10. Lomb periodogram for ERA-40 temperature and zonal wind, for zonal wave number 1 for the period 17 July to 15 September 1998. Contour lines start at 12.5 with an increment of 12.5 for each contour line.

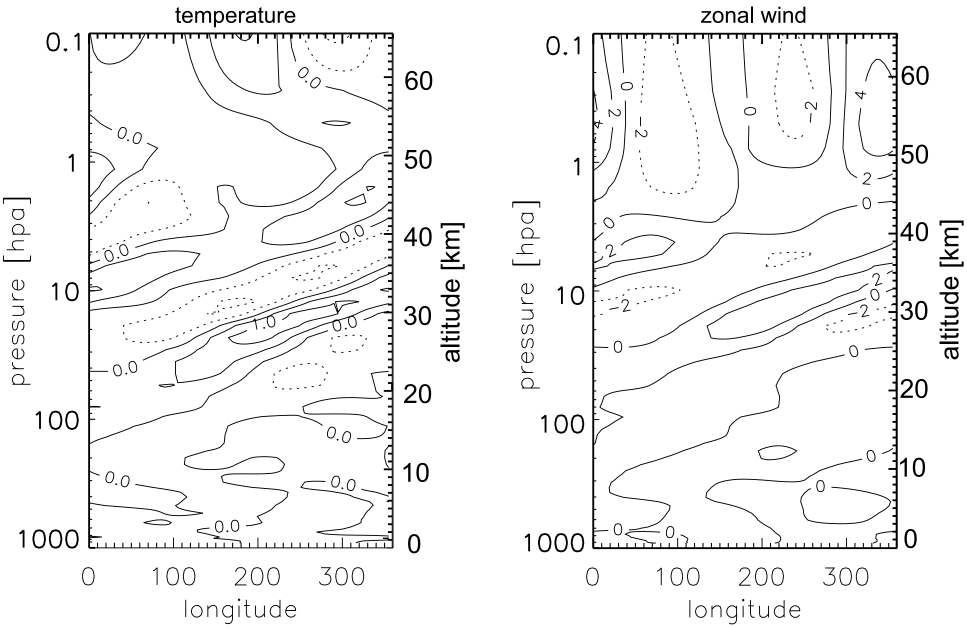

Figure 11. Pressure versus longitude plots of waves 1 and 2 in temperature and zonal wind velocity on 10 August 1998. A band-pass filter with half amplitudes at 12 and 20 days has been applied. Solid lines start at 0 K (for temperature) and 0 m/s (for zonal wind) with increments of 0.5 K and 2 m/s for each contour line. Dashed lines start at −0.5 K or −2 m/s with a decrement of 0.5 K and 2 m/s for each contour line.

wind and temperature periodograms at 15–20 hPa show a maximum around waves 1 and 2 with periods of 15 days, which is not present in the meridional wind.

[33] Figures 14 and 15 are the same as Figures 6 and 7 but now for, respectively, 1 October 2000 and longitude = 180°. The Kelvin wave induced zonal wind and temperature perturbations are up to 5 m/s and 2 K, respectively. Largest perturbations are found between 5 to 10 hPa; furthermore, large amplitudes can be found between 10 to 20 hPa, the altitude where we found maximum

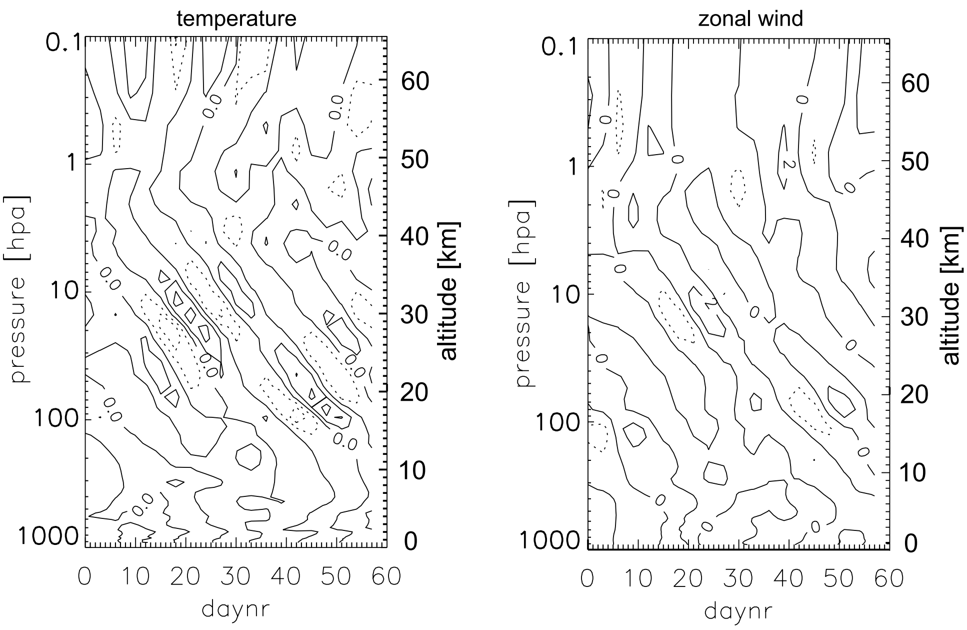

Figure 12. Pressure versus time (daynumber of the 60-day period 17 July to 15 September 1998) plots of waves 1 and 2 in temperature and zonal wind velocity at longitude = 205°. A band-pass filter with half amplitudes at 12 and 20 days has been applied. Solid lines start at 0 K (for temperature) and 0 m/s (for zonal wind) with increments of 0.5 K and 2 m/s for each contour line. Dashed lines start at −0.5 K or −2 m/s with a decrement of 0.5 K and 2 m/s for each contour line.

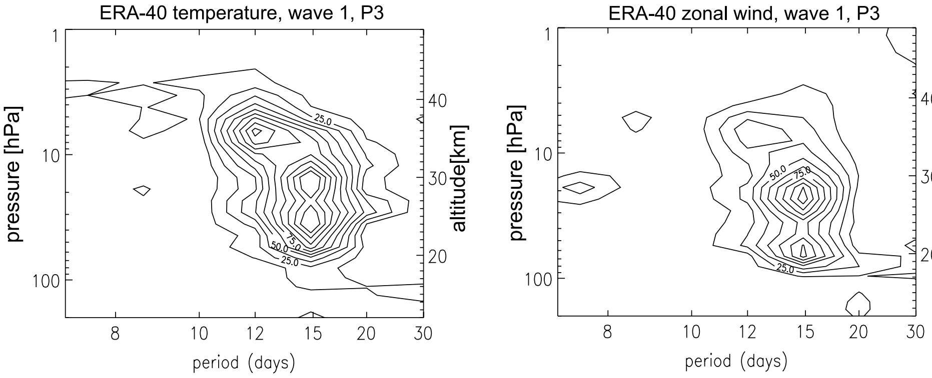

Figure 13. Lomb periodogram for ERA-40 temperature and zonal wind, for zonal wave number 1 for the period 19 September to 18 November 2000. Contour lines start at 12.5 with an increment of 12.5 for each contour line.

periodogram values. The vertical wavelength is about 10–12 km.

5. Total Ozone Column Variation Derived From ECMWF Zonal Wind and Temperature

[34] The Kelvin wave variability in the ERA-40 zonal wind and temperature show very good agreement with the Kelvin wave variability previously found in the GOME total ozone column data. Next we will examine whether the fluctuations found in the ERA-40 data theoretically can lead to the fluctuations found in the total ozone columns. First we determine the fluctuations in the ozone mixing ratio resulting from the temperature and zonal wind fluctuations. For this we use the linearized tracer continuity equation [from *Andrews et al.* 1987, equation 9.4.4.],

$$\frac{\partial \chi'}{\partial t} + \bar{u}\frac{\partial \chi'}{\partial x} + w'\frac{\partial \bar{\chi}}{\partial z} = S_P, \tag{15}$$

where χ is the tracer mixing ratio, primes denote wave perturbations, and the overbar denotes the zonal mean. The net photochemical production/destruction S_P will be neglected in the following calculation. The analyzed Kelvin wave fluctuations in the GOME ozone columns show characteristics of the slow Kelvin waves in the lower stratosphere. In the lower stratosphere, photochemical

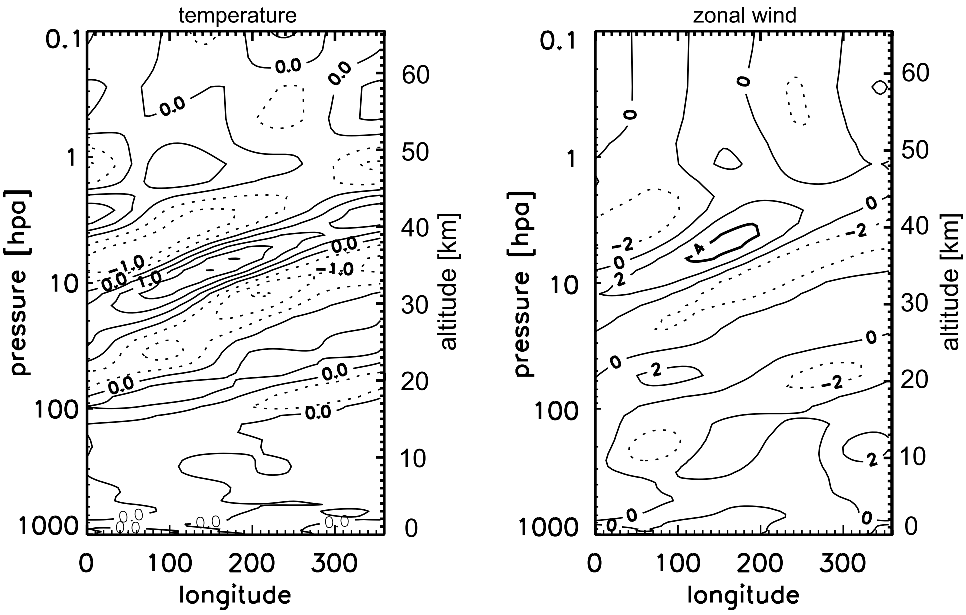

Figure 14. Pressure versus longitude plots of waves 1 and 2 in temperature and zonal wind velocity on 1 October 2000. A band-pass filter with half amplitudes at 12 and 20 days has been applied. Solid lines start at 0 K (for temperature) and 0 m/s (for zonal wind) with increments of 0.5 K and 2 m/s for each contour line. Dashed lines start at −0.5 K or −2 m/s with a decrement of 0.5 K and 2 m/s for each contour line.

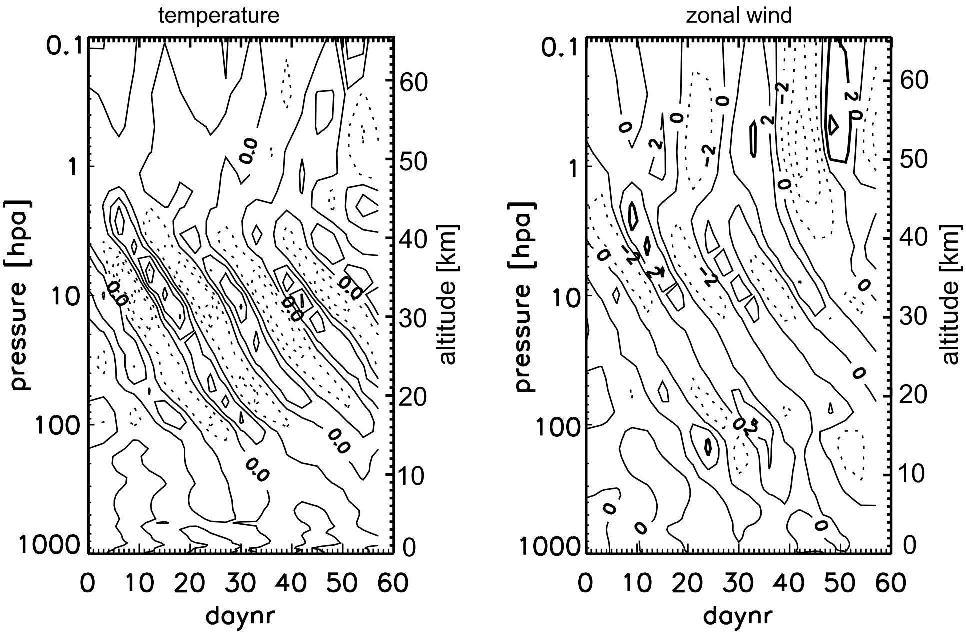

Figure 15. Pressure versus time (daynumber of the 60-day period 19 September to 18 November 2000) plots of waves 1 and 2 in temperature, zonal wind velocity at longitude = 180°. A band-pass filter with half amplitudes at 12 and 20 days has been applied. Solid lines start at 0 K (for temperature) and 0 m/s (for zonal wind) with increments of 0.5 K and 2 m/s for each contour line. Dashed lines start at −0.5 K or −2 m/s with a decrement of 0.5 K and 2 m/s for each contour line.

influences on ozone can be neglected by comparison with transport effects [*Salby et al.*, 1990].

[35] To solve χ' we also use the linearized thermodynamic equation as previously applied by *Randel* [1990], *Salby et al.* [1990], and *Kawamoto et al.* [1997],

$$\left(\frac{\partial}{\partial t} + \bar{u}\frac{\partial}{\partial x}\right)T' + w'S = 0, \tag{16}$$

where

$$S = \frac{1}{H}\left(\frac{2}{7}\bar{T} + \frac{\partial \bar{T}}{\partial z}\right) \tag{17}$$

is a background static stability parameter and the other variables as defined in section 2.3. Combining equations (16) and (15) leads to the following relation between the ozone and temperature fluctuations [*Salby et al.* 1990, equation (9)]:

$$\chi' = \frac{\frac{\partial \bar{\chi}}{\partial z}}{S} T'. \tag{18}$$

This equation states that when only considering transport effects, the induced ozone fluctuations are proportional to the vertical gradient in mean ozone and in phase with the temperature fluctuations for a positive vertical gradient of ozone. Note that, on the contrary, in the upper stratosphere where photochemical effects dominate over transport effects the ozone fluctuations are out of phase [*Salby et al.*, 1990].

[36] In Figure 16, examples of the vertical distribution of ozone fluctuations calculated from equation (18) are shown. In the calculation the temperature fluctuations found in the ERA-40 data (filtered for zonal wave numbers 1 and 2 and in time with time filter with half amplitudes at 12 and 20 days) are used. The $\partial\bar{\chi}/\partial z$ has been derived from the AFGL (Air Force Geophysical Laboratory) standard atmosphere for the tropics (see Figure 17). The largest fluctuations in ppmv are located around 30 hPa, where the vertical gradient in ozone is largest. Fluctuations in the mixing ratio of ozone above 10 hPa as can be seen in Figure 16c diminish when making the conversion to DU (see Figure 16f) and thus will not make a large contribution to the total ozone column fluctuations.

[37] Using hydrostatic equilibrium, the perturbations in the total column ozone X'_{tot} in DU are given by

$$X'_{tot} = \frac{1}{2.69 \times 10^{16}} \frac{1}{g\, m_{air}} 10^{-6} \int_0^{P_{surf}} \chi'(P)\, dP, \tag{19}$$

where $1/2.69e^{16}$ is the conversion factor from number of molecules per m^2 to DU, g is the gravitational acceleration, and m_{air} is the mass of air. The profiles chosen in Figure 16 are the profiles for each period P1, P2, and P3 that give largest amplitude of ECMWF-deduced total ozone column perturbations in DU. The ECMWF-deduced total ozone column perturbations calculated for each of these profiles, and thus the maximum ECMWF-deduced total ozone column fluctuations for each period are 0.95, 0.91, and 0.98 DU for, respectively, P1, P2, and P3. For the period P2 and P3 these maximum ECMWF-deduced fluctuations are consistent with observed fluctuations in the GOME total ozone columns of ~1 DU. The maximum GOME ozone column fluctuations in periods P2 and P3 are around 1.5 DU, a factor of 1.5 larger than the maximum ECMWF-deduced fluctuations. For P1 the discrepancy

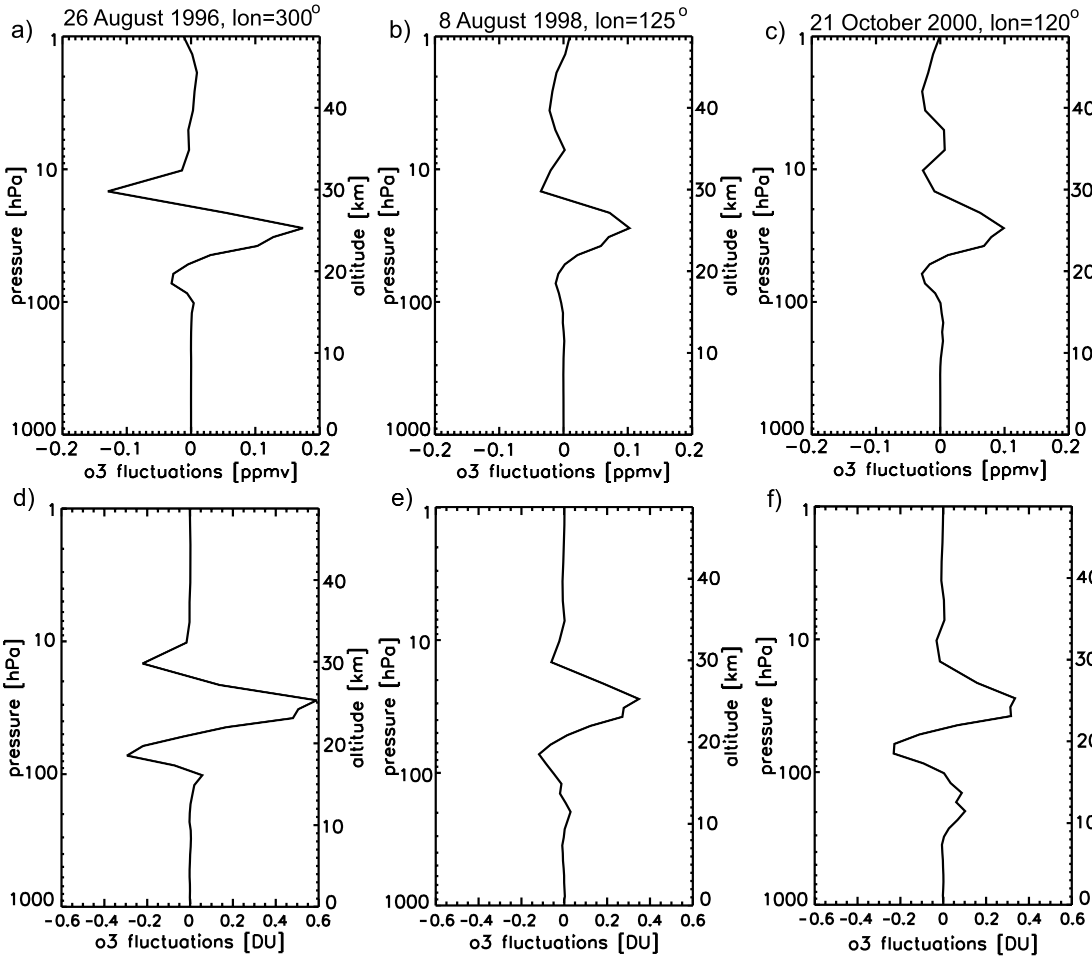

Figure 16. Vertical distribution of calculated ozone perturbations in (top) ppmv and (bottom) DU for three different date/longitude combinations: (a, d) 27 August 1996, longitude = 300°, (b, e) 8 August 1998, longitude = 125°, and (c, f) 21 October 2000, longitude = 120°.

between maximum ECMWF-deduced fluctuations and maximum GOME fluctuations is somewhat larger. The maximum ECMWF-deduced fluctuations for this period are a factor 2 smaller than the maximum GOME fluctuations of ~2 DU. We do see, however, that the amplitude of the ECMWF-deduced ozone fluctuations at 30 hPa is higher for P1 than for P2 and P3. An extended study using ozone profile measurements would be meaningful for the attribution of the cause of this discrepancy.

[38] In Figure 18 we compare the phase of ECMWF-deduced ozone column fluctuations with the fluctuations previously identified in the GOME ozone columns in T04. The figure shows longitude-time sections of the GOME and ECMWF-deduced total ozone column fluctuations for the three periods P1, P2, and P3. The added crosses indicate the timing and location of maximum GOME ozone column fluctuations. (Note that The GOME ozone column fluctuations may vary somewhat with the results in Figure 5 from T04. This is caused by the changed limits of the applied band-pass filter: 12 and 20 days compared to 10 and 15 days in T04. Furthermore, in contrary to this study, westward fluctuations have not been excluded in Figure 5 of T04.) There is a clear difference in timing of maximum fluctuations in both data sets. Also, the wave periods of

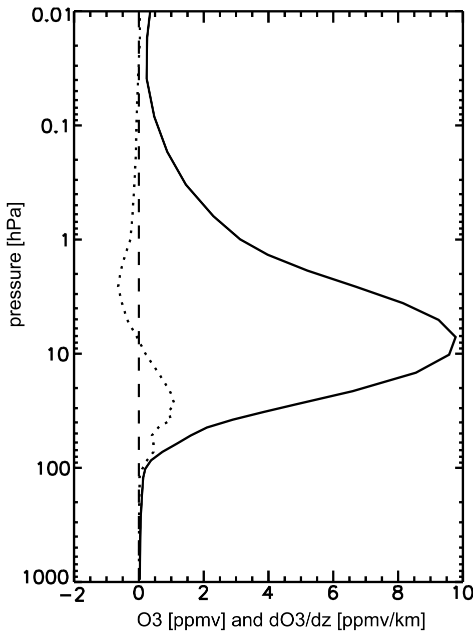

Figure 17. AFGL standard atmosphere ozone profile for the tropics (solid line) and dO_3/dz (dotted line) derived from this profile.

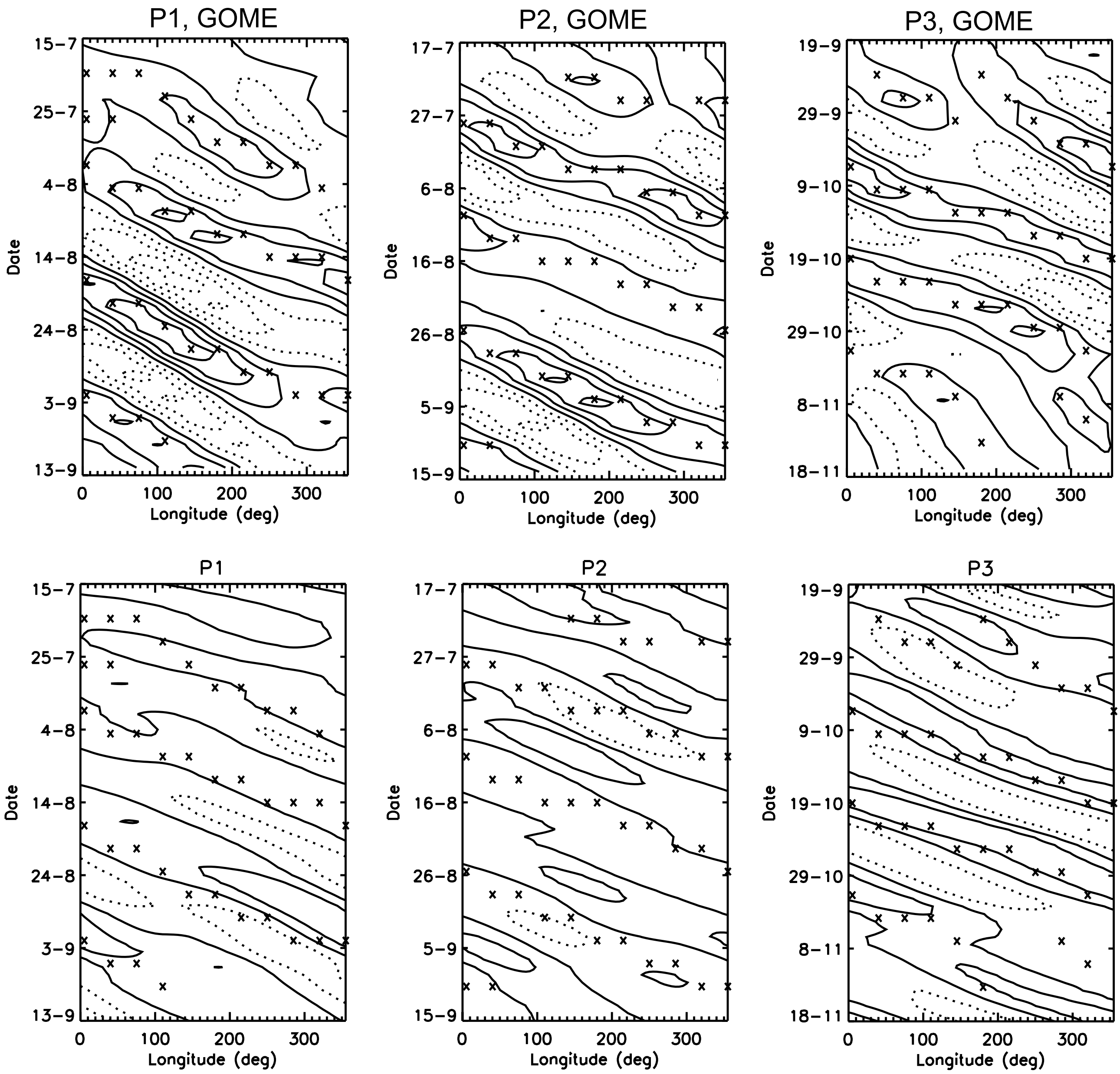

Figure 18. Longitude-time section of (top) GOME and (bottom) ECMWF-deduced total ozone columns fluctuations for periods P1, P2, and P3. Solid lines start at zero DU with an increment of 0.5 for each contour line. Dashed lines start at −0.5 DU with a decrement of 0.5 DU for each contour line. Crosses denote phase maxima of GOME ozone column fluctuations.

the GOME total ozone fluctuations seem somewhat shorter than those of the ECMWF-deduced ozone column fluctuations. These differences are an interesting outcome of this work; they might be related to a systematic error in the ECMWF data. Further study using additional data sources is needed to address the difference in timing and wave period.

[39] Figure 19 shows the pressure versus time plots of the ECMWF-deduced ozone variations for the three periods P1, P2, and P3. Downward phase propagation can be seen. The phase changes sign above ~10 hPa caused by the sign change of the vertical gradient of mean ozone at this altitude. Amplitudes are maximum around 30 hPa, as previously noted in Figure 16. The times of maximum and minimum GOME total ozone column fluctuations identified in T04 are, respectively, indicated by the solid and dashed vertical lines.

[40] We have also explored another method to derive expected total ozone column variations, i.e., by using the linearized continuity equation,

$$\frac{\partial u'}{\partial x} + \frac{\partial w'}{\partial z} = 0, \tag{20}$$

in combination with the linearized tracer continuity equation (15). The solution for u' is given by equation (11). The $\hat{u}(y)$ can be derived from the zonal wind fluctuations found in the ERA-40 data. A drawback of this method is that the information contained in the ERA-data is only used to

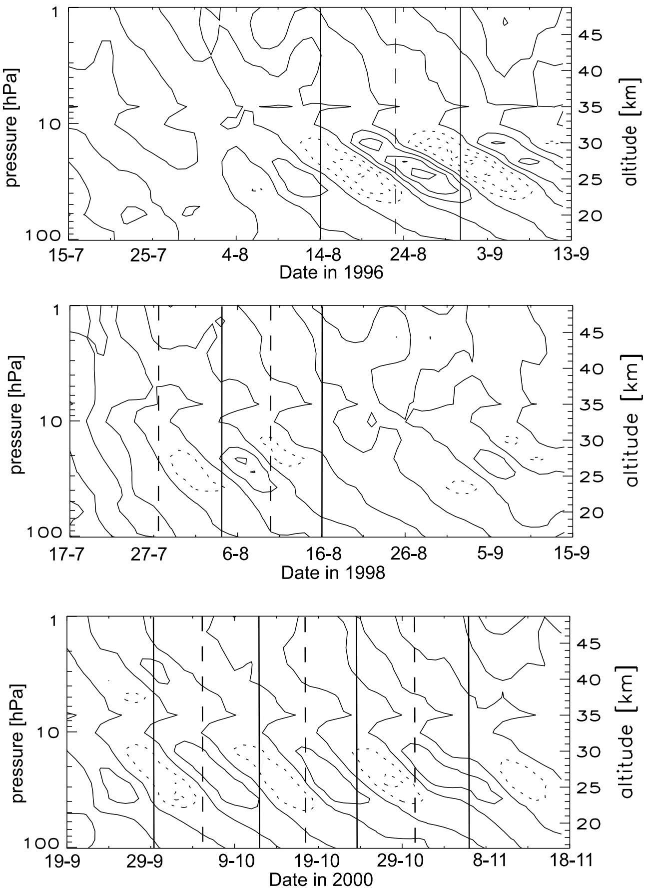

Figure 19. Pressure versus time distribution of calculated ozone perturbations in DU for (top) P1 at longitude = 300°, (middle) P2 at longitude = 125°, and (bottom) P3 at longitude = 120°. Solid contour lines start at zero DU with an increment of 0.2 for each contour line. Dotted contour lines start at −0.2 DU with a decrement of 0.2 for each contour line. Solid (dashed) vertical lines denote times of maximum (minimum) GOME ozone column variations at corresponding longitudes.

derive $\hat{u}(y)$; the information on the phase of the fluctuations in ERA-40 is not used. Furthermore, the solution for u' and through equation (20) also for w' manifests an unrealistic exponential grow with altitude because of the $e^{\frac{z}{2H}}$ factor. In reality, the wave amplitudes will not grow exponentially with altitude, owing to dissipation of the waves. These two factors make this method less suitable for drawing conclusions on, for example, phase structure of expected total ozone columns variations.

6. Conclusion and Outlook

[41] The ECMWF ERA-40 wind and temperature data provide information on the vertical structure of the Kelvin wave activity previously found in total ozone column data from GOME. Combined use of the ECMWF ERA-40 zonal wind and temperature fields and GOME total ozone column data offers the possibility to investigate the relation between Kelvin wave induced fluctuations in zonal wind, temperature, and ozone concentrations.

[42] Applying the bidimensional unequally spaced data spectral technique, introduced in T04, to the ERA-40 zonal wind and temperature data revealed spectral features that are consistent with the spectral features found in the GOME ozone columns. The spectral features correspond to Kelvin waves with wave numbers 1 and 2 and periods around 15–20 days and can be found between 100 and 10 hPa for all three high Kelvin wave activity periods identified in the GOME data (P1: 15 July to 13 September 1996; P2: 17 July to 15 September 1998; P3: 19 September to 18 November 2000). The Kelvin wave induced perturbations are up to 8 m/s for the zonal wind and 2 K for the temperature. The vertical wavelength is 10–12 km. Calculations show that the perturbations in the temperature can lead to variations in the total ozone column of around 1 DU, which is consistent with the perturbations previously found in the GOME ozone columns for periods P2 and P3. For period P1 the calculated variations are about a factor of 2 lower than observed. In these calculations we only took into account ozone fluctuations induced by horizontal and vertical transport. Ozone fluctuations induced by the temperature dependence of photochemical reactions that produce or destroy ozone are neglected, which is a good assumption in the lower part of the stratosphere. The Kelvin wave signals analyzed in this study show characteristics of lower stratospheric Kelvin waves. In this region, neglecting photochemical effects on ozone is justified.

[43] Higher up in the stratosphere the ozone fluctuations are photochemically controlled and the effect of transport on ozone is smaller [*Salby et al.*, 1990, and references therein]. We could indeed see that the transport-induced ozone fluctuations are largest below the ozone maximum, where the ozone gradient is largest, and become smaller above 40 km. The consistency between the calculated total ozone fluctuations from the zonal wind fluctuations indicates that the observed total ozone column fluctuations are indeed mainly caused by transport effects in the lower stratosphere.

[44] In this study we used the zonal wind and temperature data to retrieve information on the vertical structure of the Kelvin wave signals found in the total ozone column measurements from GOME. For a more extensive and accurate determination of the vertical distribution of the Kelvin wave signals, we need ozone profile measurements with an adequate vertical resolution. Both ozone profiles derived from the GOME nadir measurements [*van der A et al.*, 2002] and the SCIAMACHY (Scanning Imaging Absorption Spectrometer for Atmospheric Chartography) [*Bovensmann et al.*, 1999] limb measurements will be analyzed for this purpose in future work. The latter provides ozone profile data with a vertical resolution of ~3 km. The instrument performs nadir column and limb profile measurements within 7 min of each other. The combination of these measurements will offer a good possibility for studying both the horizontal and vertical distribution of Kelvin wave activity.

[45] **Acknowledgments.** The author would like to acknowledge the European Centre for Medium-Range Weather Forecasts for providing the ERA-40 data. GOME ozone products have been provided by DFD-DLR on behalf of ESA. Part of this work has been undertaken by the financial support of the Netherlands Agency for Aerospace Programs (NIVR). Furthermore, the authors would like to thank Arjo Segers (KNMI) for his assistance in the data access and handling.

References

Andrews, D. G., J. R. Holton, and C. B. Leovy (1987), *Middle Atmosphere Dynamics*, Elsevier, New York.

Bovensmann, H., J. P. Burrows, M. Buchwitz, J. Frerick, S. Noël, V. V. Rozanov, K. V. Chance, and A. P. H. Goede (1999), SCIAMACHY: Mission objectives and measurement modes, *J. Atmos. Sci.*, *56*, 127–150.

Canziani, P. O. (1999), Slow and ultraslow equatorial Kelvin waves: The UARS-CLAES view, *Q. J. R. Meteorol. Soc.*, *125*, 657–676.

Canziani, P. O., J. R. Holton, E. Fishbein, L. Froidevaux, and J. W. Waters (1994), Equatorial Kelvin waves: A UARS-MLS view, *J. Atmos. Sci.*, *51*, 3053–3076.

Canziani, P. O., J. R. Holton, E. Fishbein, and L. Froidevaux (1995), Equatorial Kelvin wave variability during 1992 and 1993, *J. Geophys. Res.*, *100*, 5193–5202.

Fujiwara, M., and M. Takahashi (2001), Role of the equatorial Kelvin wave in stratosphere-troposphere exchange in a general circulation model, *J. Geophys. Res.*, *106*, 22,763–22,780.

Fujiwara, M., K. Kita, and T. Ogawa (1998), Stratosphere-troposphere exchange of ozone associated with the equatorial Kelvin wave as observed with ozonesondes and rawinsondes, *J. Geophys. Res.*, *103*, 19,173–19,182.

Fujiwara, M., M. Hasebe, M. Shiotani, N. Nishi, H. Voemel, and S. J. Oltmans (2001), Water vapor control at the tropopause by the equatorial Kelvin wave observed over Galapagos, *Geophys. Res. Lett.*, *28*, 3143–3146.

Holton, J. R. (1992), *An Introduction to Dynamic Meteorology*, third ed., Elsevier, New York.

Kawamoto, N., M. Shiotani, and J. C. Gille (1997), Equatorial Kelvin waves and corresponding tracer oscillations in the lower stratosphere as seen in LIMS data, *J. Meteorol. Soc. Jpn.*, *75*, 763–773.

Mote, P. W., and T. J. Dunkerton (2002), Kelvin waves in stratospheric temperature observed by the Microwave Limb Sounder, *J. Geophys. Res.*, *107*(D14), 4218, doi:10.1029/2001JD001056.

Mote, P. W., and T. J. Dunkerton (2004), Kelvin wave signatures in stratospheric trace constituents, *J. Geophys. Res.*, *109*, D03101, doi:10.1029/2002JD003370.

Murakami, M. (1979), Large scale aspects of deep convective activity over the GATE area, *Mon. Weather Rev.*, *107*, 994–1013.

Pawson, S., and M. Fiorino (1998), A comparison of reanalyses in the tropical stratosphere: 1. Thermal structure and the annual cycle, *Clim. Dyn.*, *14*, 631–644.

Press, W. H., S. A. Teukolsky, W. T. Vetterling, and B. P. Flannery (1992), *Numerical Recipes in Fortran (or in C or in Pascal): The Art of Scientific Computing*, second ed., Cambridge Univ. Press, New York.

Randel, W. J. (1990), Kelvin wave-induced trace constituent oscillations in the equatorial stratosphere, *J. Geophys. Res.*, *95*, 18,641–18,652.

Randel, W. J., and J. C. Gille (1991), Kelvin wave variability in the upper stratosphere observed in SBUV ozone data, *J. Atmos. Sci.*, *48*, 2336–2349.

Salby, M. L., D. L. Hartmann, P. L. Bailey, and J. C. Gille (1984), Evidence for equatorial Kelvin modes in Nimbus-7 LIMS, *J. Atmos. Sci.*, *41*, 220–235.

Salby, M. L., P. Callaghan, S. Solomon, and R. Garcia (1990), Chemical fluctuations associated with vertically propagating equatorial Kelvin waves, *J. Geophys. Res.*, *95*, 20,491–20,505.

Scargle, J. D. (1982), Studies in astronomical time series analysis: II. Statistical aspects of spectral analysis of unevenly spaced data, *Astrophys. J.*, *263*, 835–853.

Shiotani, M., J. C. Gille, and A. E. Roche (1997), Kelvin waves in the equatorial lower stratosphere as revealed by cryogenic limb array etalon spectrometer temperature data, *J. Geophys. Res.*, *102*, 26,131–26,140.

Simmons, A. J., and J. K. Gibson (2000), The ERA-40 project plan, *ERA-40 Proj. Rep. Ser. 1*, Eur. Cent. for Medium-Range Weather Forecasts, Reading, UK.

Stone, E. M., et al. (1995), Space-time integrity of improved stratospheric and mesospheric sounder and Microwave Limb Sounder temperature fields at Kelvin wave scales, *J. Geophys. Res.*, *100*, 14,089–14,096.

Straub, K. H., and G. N. Kiladis (2002), Observations of a convectively coupled Kelvin wave in the eastern Pacific ITCZ, *J. Atmos. Sci.*, *59*, 30–53.

Timmermans, R. M. A., R. F. van Oss, and H. M. Kelder (2004), Equatorial Kelvin Wave signatures in ozone column measurements from Global Ozone Monitoring Experiment (GOME), *J. Geophys. Res.*, *109*(D1), D01101, doi:10.1029/2003JD003946.

Tindall, J. C. (2003), Dynamics of the tropical tropopause and lower stratosphere, Ph.D. thesis, Dep. of Meteorol., Univ. of Reading, Reading, UK.

Tindall, J. C., J. Thuburn, and E. J. Highwood (2005a), Equatorial waves in the lower stratosphere: 1. A novel detection method, *Q. J. R. Meteorol. Soc.*, in press.

Tindall, J. C., J. Thuburn, and E. J. Highwood (2005b), Equatorial waves in the lower stratosphere: 2. Annual and interannual variability, *Q. J. R. Meteorol. Soc.*, in press.

van der A, R. J., R. F. van Oss, A. J. M. Piters, J. P. F. Fortuin, Y. J. Meijer, and H. M. Kelder (2002), Ozone profile retrieval from recalibrated global ozone monitoring experiment data, *J. Geophys. Res.*, *107*(D15), 4239, doi:10.1029/2001JD000696.

Wallace, J. M., and V. E. Kousky (1968), Observational evidence of Kelvin waves in the tropical stratosphere, *J. Atmos. Sci.*, *25*, 900–907.

Ziemke, J. R., and J. L. Stanford (1994), Kelvin waves in total column ozone, *Geophys. Res. Lett.*, *21*, 105–108.

H. M. Kelder, R. M. A. Timmermans, and R. F. van Oss, Royal Netherlands Meteorological Institute, PO Box 201, 3730 AE De Bilt, Netherlands. (renske.timmermans@knmi.nl)

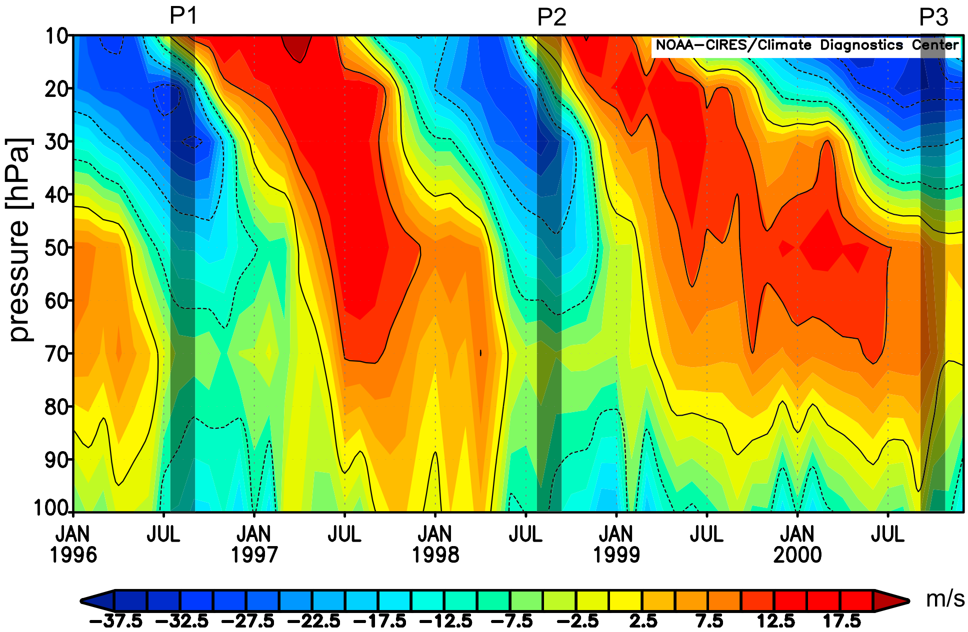

Figure 1. Monthly mean zonal wind (m/s) at the equator and 105° E for January 1996 to December 2000 and pressure levels between 100 and 10 hPa. (Image provided by the NOAA-CIRES Climate Diagnostics Center, Boulder, Colorado, USA, from their Web site at http://www.cdc.noaa.gov/.)

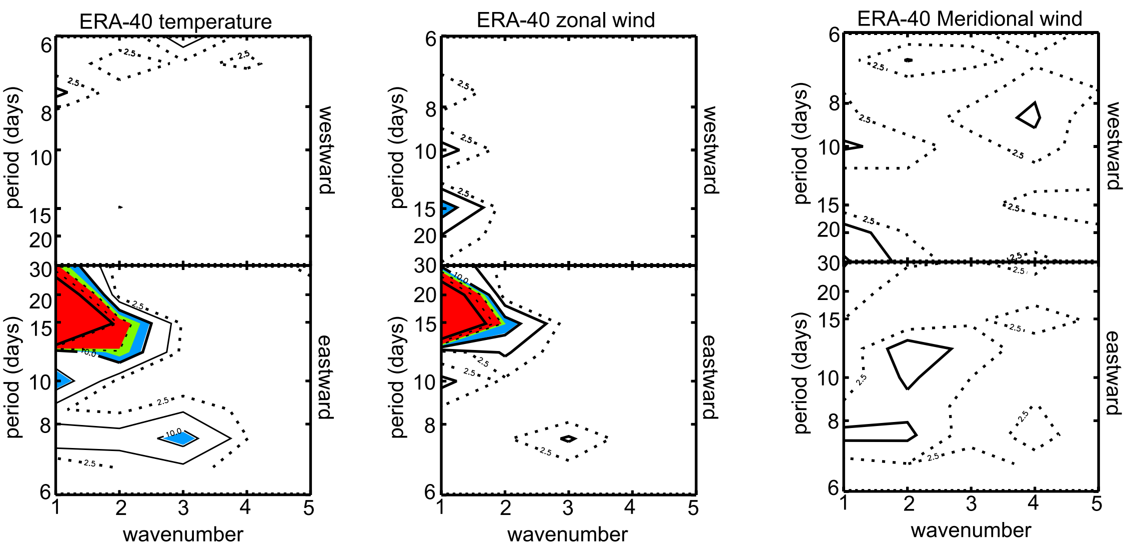

Figure 2. Lomb periodogram for ERA-40 temperature and zonal and meridional wind at 15 hPa for the period 15 July to 13 September 1996. Contour lines start at 2.5, followed by contour lines at 5, 10, 15, 20 and 25. The blue, green, and red areas, respectively, denote the 90%, 99%, and 99,9% significant signals.

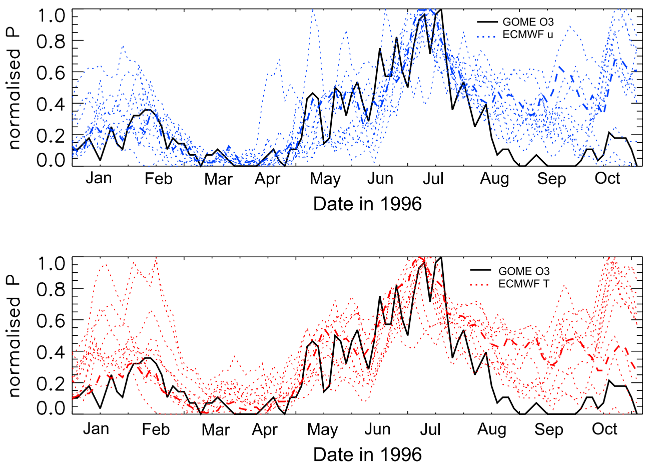

Figure 9. Normalized ozone column periodogram values P_N (solid line) and (top) normalized zonal wind and (bottom) temperature periodogram values, calculated over 60-day time periods, for wave 1 with a wave period of 15 days, as function of the starting day of the 60-day periods in 1996. The zonal wind and temperature periodograms are calculated on 11 different levels (dotted lines) between 80 hPa and 8 hPa. The thick dashed lines are the periodogram values on the 15-hPa level.